ACS chemical biology

Articles

pubs.acs.org/acschemicalbiology

Isolation and Functional Characterization of Peptide Agonists of PTPRJ, a Tyrosine Phosphatase Receptor Endowed with Tumor Suppressor Activity

Francesco Paduano,[†] Francesco Ortuso,[‡] Pietro Campiglia,[§] Cinzia Raso,[†] Enrico Iaccino,[†] Marco Gaspari,[†] Eugenio Gaudio,[†,∥] Graziella Mangone,[†] Alfonso Carotenuto,[⊥] Anna Bilotta,[†] Domenico Narciso,[†] Camillo Palmieri,[†] Valter Agosti,[†] Anna Artese,[‡] Isabel Gomez-Monterrey,[⊥] Marina Sala,[§] Giovanni Cuda,[†] Rodolfo Iuliano,[†] Nicola Perrotti,[†] Giuseppe Scala,[†] Giuseppe Viglietto,[†] Stefano Alcaro,[‡] Carlo M. Croce,[∥] Ettore Novellino,[⊥] Alfredo Fusco,[¶] and Francesco Trapasso*[,†]

[†]Dipartimento di Medicina Sperimentale e Clinica, Università "Magna Græcia" di Catanzaro, Campus "S. Venuta", 88100 Catanzaro, Italy

[‡]Laboratorio di Chimica Farmaceutica Computazionale, Dipartimento di Scienze Farmacobiologiche, Università "Magna Græcia" di Catanzaro, Campus "S. Venuta", 88100 Catanzaro, Italy

[§]Dipartimento di Scienze Farmaceutiche e Biomediche, Sezione Chimico-Tecnologica, Università di Salerno, 84084 Fisciano (Salerno), Italy

[∥]Department of Molecular Virology, Immunology and Medical Genetics and Comprehensive Cancer Center, The Ohio State University, Columbus, Ohio 43210, United States

[⊥]Dipartimento di Chimica Farmaceutica e Tossicologica, Università degli Studi di Napoli "Federico II", 80131 Naples, Italy

[¶]Dipartimento di Biologia e Patologia Cellulare e Molecolare c/o Istituto di Endocrinologia ed Oncologia Sperimentale del CNR, Università degli Studi di Napoli "Federico II", 80131 Naples, Italy

Supporting Information

ABSTRACT: PTPRJ is a receptor-type protein tyrosine phosphatase whose expression is strongly reduced in the majority of investigated cancer cell lines and tumor specimens. PTPRJ negatively interferes with mitogenic signals originating from several oncogenic receptor tyrosine kinases, including HGFR, PDGFR, RET, and VEGFR-2. Here we report the isolation and characterization of peptides from a random peptide phage display library that bind and activate PTPRJ. These agonist peptides, which are able to both circularize and form dimers in acqueous solution, were assayed for their biochemical and biological activity on both human cancer cells and primary endothelial cells (HeLa and HUVEC, respectively). Our results demonstrate that binding of PTPRJ-interacting peptides to cell cultures dramatically reduces the extent of both MAPK phosphorylation and total phosphotyrosine levels; conversely, they induce a significant increase of the cell cycle inhibitor $p27^{Kip1}$. Moreover, PTPRJ agonist peptides both reduce proliferation and trigger apoptosis of treated cells. Our data indicate that peptide agonists of PTPRJ positively modulate the PTPRJ activity and may lead to novel targeted anticancer therapies.

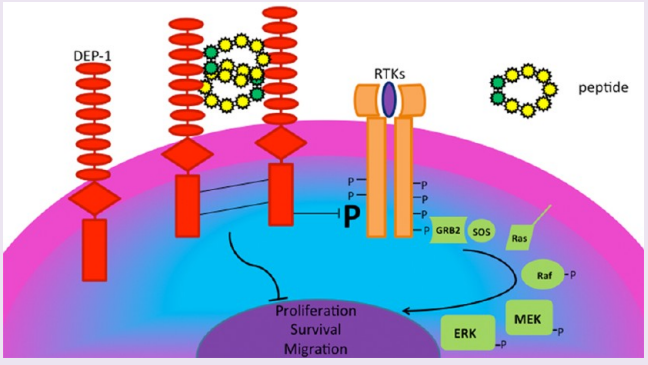

Among all protein tyrosine phosphatases,[1] PTPRJ is of particular interest for its role in human and experimental tumorigenesis.[2] In fact, after its discovery,[3,4] a consistent body of literature supports its tumor suppressor activity in several models. PTPRJ (also named DEP-1, HPTPη, or CD148) is down-regulated in mammary cancer cells, and its restoration blocks their proliferation;[5] a similar behavior was described in both human and experimental models of thyroid tumorigenesis, where PTPRJ overexpression was able to interfere with cancer cells malignant phenotype both *in vitro* and *in vivo*.[6,7] Moreover, down-regulation of PTPRJ expression operated by miR-328 increases cell proliferation in HeLa and SKBr3 cell lines.[8] *PTPRJ* has been successfully used as a therapeutic gene in cancer gene therapy preclinical models of thyroid and pancreatic cancer.[9,10] The role of PTPRJ in human tumorigenesis was also highlighted by Ruivenkamp and colleagues,[11,12]

Received: February 3, 2012
Accepted: July 3, 2012
Published: July 3, 2012

who demonstrated that *PTPRJ* was affected by loss of heterozygosity (LOH) in colon, lung, and mammary tumors; a significant percentage of LOH was also described in human thyroid tumors.[13] Moreover, a polymorphism in the mouse *Ptprj* locus (*Scc1*) is associated with colon cancer development,[11] although *Ptprj* genetic ablation did not induce spontaneous tumors in mice.[14,15]

The biochemical pathways negatively regulated by PTPRJ have been partly elucidated. Various reports indicate an inhibitory effect of PTPRJ on several players of the mitogenic signals in both normal and cancer cells. In fact, PTPRJ interacts with and dephosphorylates numerous receptor tyrosine kinases (RTKs) including PDGFR, HGFR, RET, and EGFR,[16−19] whose aberration in cancer cells is responsible for self-sufficiency cell growth.[20] PTPRJ is also a negative modulator of the signaling mediated by cytosolic transducers, including phospholipase Cγ1 (PLCγ1), LAT, PKB/Akt, and PI3K.[21−23] Noteworthy, the role of PTPRJ on the inhibition of RTKs was also extended to VEGFR-2,[24,25] whose activity is required for the formation of new vessels in tumor progression. Lately, PTPRJ ligands have been discovered; they include the heparan sulfate proteoglycan Syndecan-2 (S2ED)[26] and Thrombospondin-1 (TSP1).[27] PTPRJ acts as key intermediary in S2ED-mediated cell adhesion, by modulating downstream β1 integrin-mediated adhesion and cytoskeletal organization, whereas TSP1, a glycoprotein that mediates cell−cell and cell−matrix interactions, increases PTPRJ activity, influencing the dephosphorylation of its substrates.

These findings make PTPRJ an interesting candidate for the generation of novel therapeutic strategies. In fact, a PTPRJ monoclonal antibody was able to induce both ERK1/2 dephosphorylation and cell growth inhibition *in vitro* as well as *in vivo* inhibition of angiogenesis.[28]

Here, we describe the isolation and characterization of synthetic peptides that interact with PTPRJ ectodomain and are able to trigger its signaling. We identified PTPRJ-binding peptides from a combinatorial phage display library in a cell-free assay; two peptides, whose specificity was tested *in vitro*, were responsible of both biochemical and biological PTPRJ-mediated effects, as we observed both dephosphorylation of PTPRJ targets and cell growth inhibition of HeLa and HUVEC cells. Our results point to the selected peptides as interesting lead compounds for the development of a novel class of effective chemotherapeutic agents.

RESULTS AND DISCUSSION

Isolation of PTPRJ-Binding Peptides by Phage Display. To isolate PTPRJ ligands, we screened a 9-mer cyclic random phage display library against a PTPRJ-tagged recombinant protein. A schematic representation of the experimental approach is shown in Figure 1. Briefly, a recombinant adenovirus carrying a *PTPRJ* cDNA, modified at its 3′-end with a sequence coding for a six-histidine tag, was used to infect recipient A549 cells. Four days after infection, A549-transduced cells were lysed and cell membranes enriched to improve the purification of mature integral proteins. PTPRJ-His6 protein was isolated from protein lysates by poly(His)-avid magnetic beads. These beads, conjugated with PTPRJ-His6, were then incubated with the phage display library. After three rounds of panning, we isolated by immunoscreening 25 phage clones reactive against the PTPRJ-His6 recombinant protein; physical interaction between isolated phages and PTPRJ-His6 was also confirmed by ELISA. Phage DNAs were purified and sequenced to establish the sequence of peptides interacting with PTPRJ-His6. Among the isolated clones, three of them (PTPRJ-pep19, PTPRJ-pep23, and PTPRJ-pep24) were further investigated based on the ELISA absorbance (Table 1).

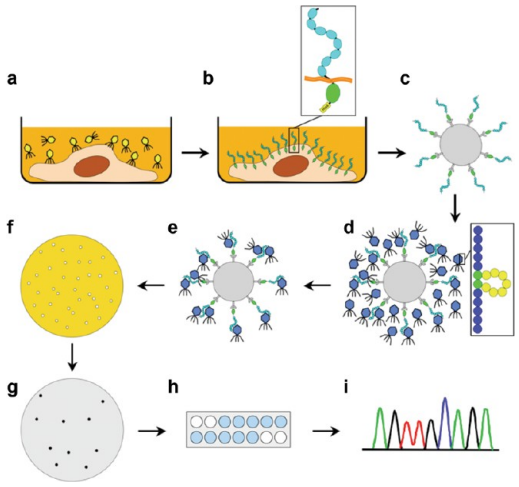

Figure 1. Schematic representation of the experimental cell-free approach used to isolate PTPRJ-interacting peptides. (a) A549 lung cancer cells were infected with a recombinant adenovirus carrying *PTPRJ*-His6 as a transgene. (b) A549 cells overexpressing the recombinant PTPRJ-His6 protein were lysed, and (c) PTPRJ-His was isolated from enriched membranes by poly(His)-avid magnetic beads. (d) PTPRJ-His6-conjugated beads were used to screen a phage display library. (e) PTPRJ-His6-interacting phages were eluted and (f) plated onto Petri dishes. (g) Plaques were transferred on a membrane and hybridized to PTPRJ-His6. (h) Plaques positive to immuno-screening were then confirmed by ELISA. (i) Genomic DNAs from positive phages were sequenced for peptides identification.

Table 1. Peptide Ligands Isolated from a C7C Phage Display Library[a]

peptide sequence	phage clones	ELISA absorbance
CNSHNHHTC	PTPRJ-pep5	0.055
CHHNLTHAC	PTPRJ-pep19	0.248
CLKQLQRGC	PTPRJ-pep23	0.143
CLHHYHGSC	PTPRJ-pep24	0.330
CTLYHNAGC	PTPRJ-scrambled	

[a]Peptide sequence of phage clones (N-term to C-term). ELISA absorbance values of single phage clones were expressed as the difference between $OD_{405\ nm}$ and $OD_{629\ nm}$.

This approach was performed after our first attempt to isolate PTPRJ-specific ligands by biopanning on living cells.[29,30] In fact, by using this method we isolated a few clones, all of them carrying a redundant sequence (PTPRJ-pep5; Table 1). Therefore, to expand the number of candidate PTPRJ agonists, we have been forced to the cell-free approach described above.

Peptide sequences obtained from both experiments were compared against protein databases; no *in silico* similarities have been observed with known proteins, either soluble or structural (data not shown).

Circularization and Stability of Peptides Putatively Interacting with PTPRJ. Before testing the biological effects of newly isolated PTPRJ-interacting peptides on living cells, we analyzed their circularization by mass spectrometry. Analysis by matrix-assisted laser desorption ionization mass spectrometry

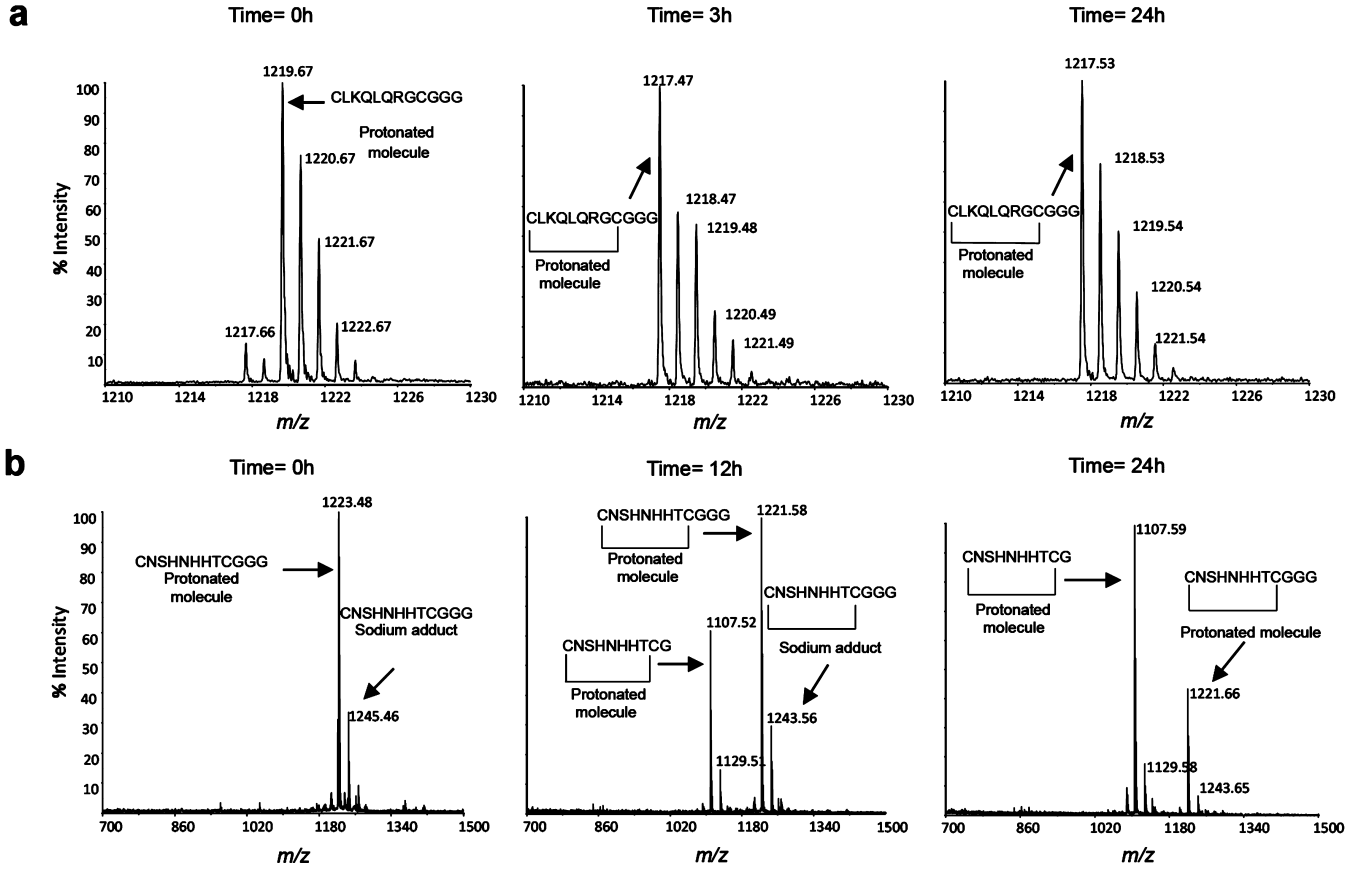

Figure 2. Circularization and stability of representative peptides putatively interacting with PTPRJ. (a) MALDI-TOF spectra of PTPRJ-pep23 acquired: (0 h) immediately after resuspension in buffer; (3 h) 3 h after reconstitution; (24 h) 24 h after reconstitution. From the isotopic pattern obtained in spectrum (24 h), it was estimated that, after 24 h, over 85% of the peptide was present in its oxidized form (m/z 1217.5). (b) MALDI-TOF spectra of cell suspension medium taken from HeLa cells incubated with peptide PTPRJ-pep5 acquired: (0 h) immediately after its addition to the suspension medium (the peptide was detected at m/z 1223.48 corresponding to its reduced form); (12 h) after 12 h in cell suspension medium; m/z 1221.58 corresponds to the cyclic form of the peptide, whereas the peak at 1107.52 may be attributed to proteolytic loss of the two C-ter glycines; (24 h) after 24 h in cell suspension medium; the spectrum suggests an increase in relative abundance of the proteolytic product.

showed that peptides PTPRJ-pep5, PTPRJ-pep19, PTPRJ-pep23, and PTPRJ-pep24 were in a cyclic conformation, bearing an intramolecular disulfide bridge; cyclic conformation was reached 3 h after reconstitution of the peptides in PBS and remained stable over 24 h. The stability of peptides putatively interacting with PTPRJ was also assessed through mass spectrometry; peptides PTPRJ-pep5, PTPRJ-pep19, PTPRJ-pep23, and PTPRJ-pep24 were stable in cell culture medium in presence of HeLa cells up to 24 h after their reconstitution. MALDI-TOF spectra of PTPRJ-pep23 (Figure 2a) and PTPRJ-pep5 (Figure 2b) are reported as representative experiments of circularization and stability, respectively.

PTPRJ Synthetic Peptides Partly Inhibit Cell Growth and Induce Apoptosis of HeLa Cancer Cells and HUVEC Endothelial Cells. We investigated if treatment of HeLa and HUVEC cells, both expressing endogenous PTPRJ (Figure 3a), with PTPRJ-interacting peptides could result in any biological effect. To this purpose, cells were exposed to 160 μM PTPRJ-pep5, PTPRJ-pep19, PTPRJ-pep23, and PTPRJ-pep24 and counted after a 48 h period of recovery. Both cell types showed a 20% reduction of their cell number compared to scrambled peptide following PTPRJ-pep19 and PTPRJ-pep24 administration. No modifications were observed in cells treated with both PTPRJ-pep5 and PTPRJ-pep23 compared to scrambled peptide (Figure 3b).

To assess the importance of circularization on PTPRJ peptides activity, similar experiments were performed by using PTPRJ-pep19 in which circularization was abrogated by the replacement of the terminal cysteines involved in the intramolecular disulfide bridge with serine residues (PTPRJ-pep19-linear). No effects were observed after treatment with such a modified peptide compared to its native peptide, demonstrating that PTPRJ peptides activity strongly depends upon its circular state (Figure 3b).

We also evaluated cell cycle modifications induced by PTPRJ-pep19 and PTPRJ-pep24 on HeLa and HUVEC cells. Forty-eight hours after recovery, cells were analyzed by propidium iodide staining and flow cytometric analysis. Treatment with candidate PTPRJ agonist peptides resulted in the presence of a sub-G1 population, suggestive of apoptotic cell death. Peaks accounting for 15.7% and 15% of the overall cell population were detectable in HeLa cancer cells treated with PTPRJ-pep19 and PTPRJ-pep24, respectively (Figure 3c, left panel). Similar results were also obtained in HUVEC cells, where the administration of PTPRJ-pep19 and PTPRJ-pep24 peptides was able to trigger cell death of 14.9% and 12.1% of cells, respectively (Figure 3c, right panel). Conversely, no sub-G1 populations were observed in both cell lines exposed to scrambled peptides.

dx.doi.org/10.1021/cb300281t | ACS Chem. Biol. 2012, 7, 1666–1676

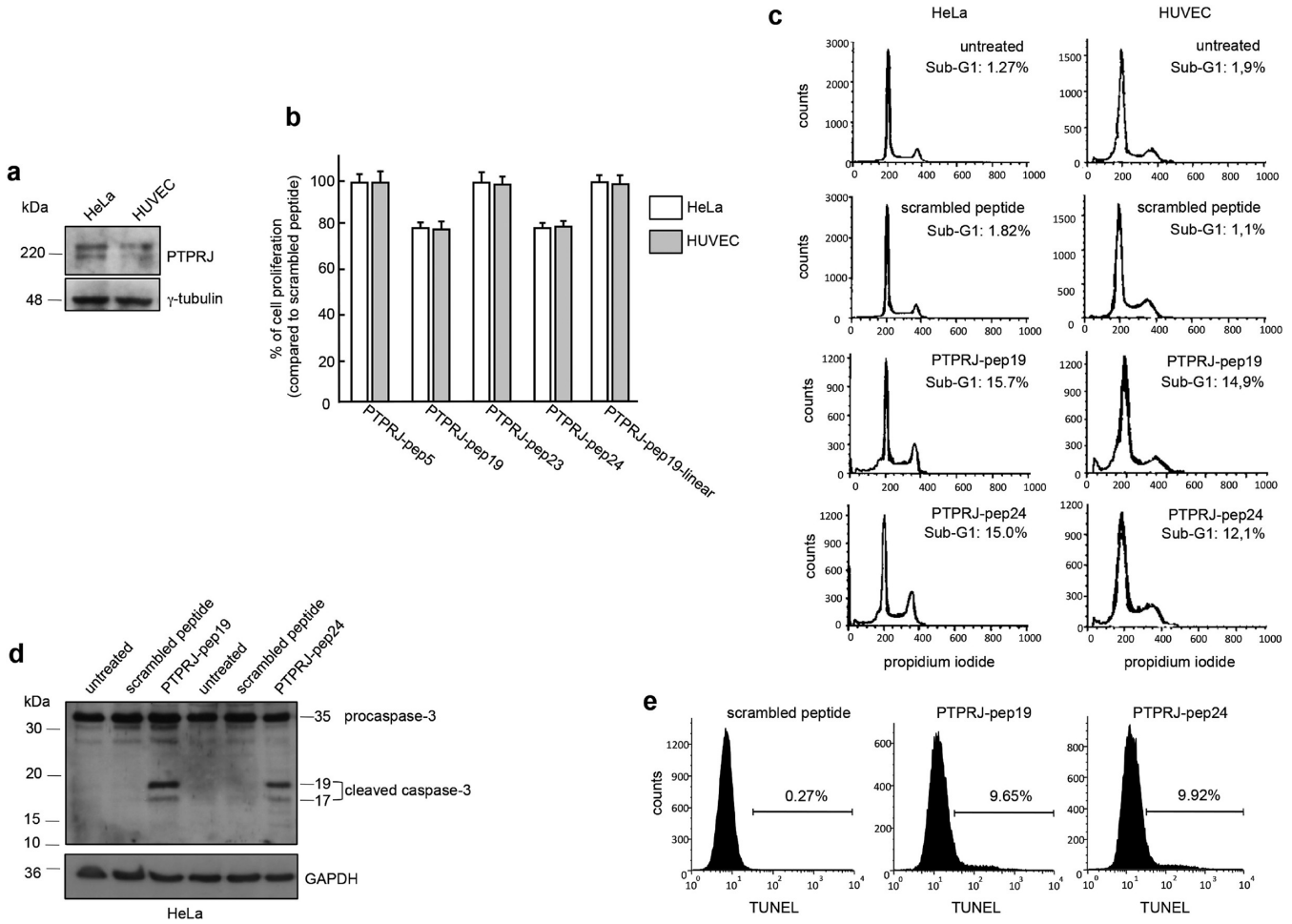

Figure 3. Cell growth inhibition and cell death induced by PTPRJ-peptides in HeLa cancer cells and in HUVEC endothelial cells. (a) Endogenous PTPRJ protein expression in HeLa and HUVEC cells. Expression was normalized on γ-tubulin. (b) Cell growth inhibition induced by PTPRJ-pep5, PTPRJ-pep19, PTPRJ-pep23, PTPRJ-pep24, and PTPRJ-pep19-linear peptides in HeLa cells (white columns) and HUVEC cells (gray columns). The relative cell growth (as percentage of the growth observed in scrambled peptide-treated cells) of HeLa and HUVEC cells at recovery of 48 h after 24 h exposure to 160 μM PTPRJ peptides. Data represent the mean values ± SD of at least three independent experiments. (c) PTPRJ-pep19 and PTPRJ-pep24 induced cell death of HeLa and HUVEC cells. Flow cytometric detection of apoptosis of HeLa (left panel) and HUVEC (right panel) cells at 48 h recovery after 24 h exposure to 160 μM PTPRJ-pep19, PTPRJ-pep2,4 and scrambled peptide. The percentage of sub-G1 population is reported in each histogram. (d) PTPRJ-pep19 and PTPRJ-pep24 peptides induced cleavage of caspase-3 in HeLa cancer cells. HeLa cells were treated with 160 μM PTPRJ-pep19, PTPRJ-pep24, and scrambled peptide and analyzed at 48 h. Total and active caspase-3 were detected by specific antibodies, and expression was normalized on GAPDH. (e) Treatments of HeLa cells with PTPRJ peptides showed induction of apoptosis. HeLa cells were treated with 160 μM PTPRJ-pep19, PTPRJ-pep24, and scrambled peptide and analyzed at 48 h by TUNEL assay.

To confirm apoptosis induced by PTPRJ peptides in HeLa cells, caspase-3 activation was analyzed by Western blot by detecting active caspase-3. Following incubation of HeLa cells with 160 μM of PTPRJ-pep19 and PTPRJ-pep24, cleaved products of caspase-3 were detected at 48 h. Conversely, in either untreated or scrambled peptide treated cells no active caspase-3 was detected (Figure 3d). Apoptosis of HeLa cells was further confirmed by TUNEL assay; as shown in Figure 3e, 160 μM PTPRJ-pep19 and PTPRJ-pep24 induced apoptosis in HeLa cells at 48 h with respect to cell treated with scrambled peptide (9.65% or 9.92% versus 0.27%, respectively).

PTPRJ Synthetic Peptides Negatively Modulate ERK1/2 Phosphorylation and Increase p27 Protein Levels. Several reports indicate that PTPRJ reduces the phosphorylation extent of ERK1/2, thus negatively modulating MAPK signaling.[7,9,31] Short-term treatment of HeLa and HUVEC cells with 160 μM PTPRJ-pep19 and PTPRJ-pep24 resulted in a dramatic reduction of ERK1/2 phosphorylation; this dephosphorylation was observed already 15 min after treatment (Figure 4a). Conversely, ERK1/2 phosphorylation status was unchanged when cells were treated with either scrambled peptide or PTPRJ-pep5 and PTPRJ-pep23 (data not shown). We also evaluated the ability of PTPRJ-pep19 and PTPRJ-pep24 to interfere with the pattern of tyrosine phosphorylation in both HeLa and HUVEC cells; treatment of both cell lines with PTPRJ-pep24 resulted in the presence of hypophosphorylated bands (Figure 4b) compared to cell lysates extracted from cells treated with PTPRJ-pep5 and PTPRJ-pep23 where no changes of the tyrosine phosphorylation pattern was detected (data not shown); similar results were obtained with PTPRJ-pep19 (data not shown).

In addition, we checked PTPRJ signaling in NIH3T3 cells expressing exogenous PTPRJ. NIH3T3 is a mouse cell line lacking endogenous Ptprj protein (Figure 4c).[14] The addition of PTPRJ-pep19 and PTPRJ-pep24 to NIH3T3 did not change the phosphorylation state of ERK (Figure 4d, left panel).

dx.doi.org/10.1021/cb300281t | ACS Chem. Biol. 2012, 7, 1666–1676

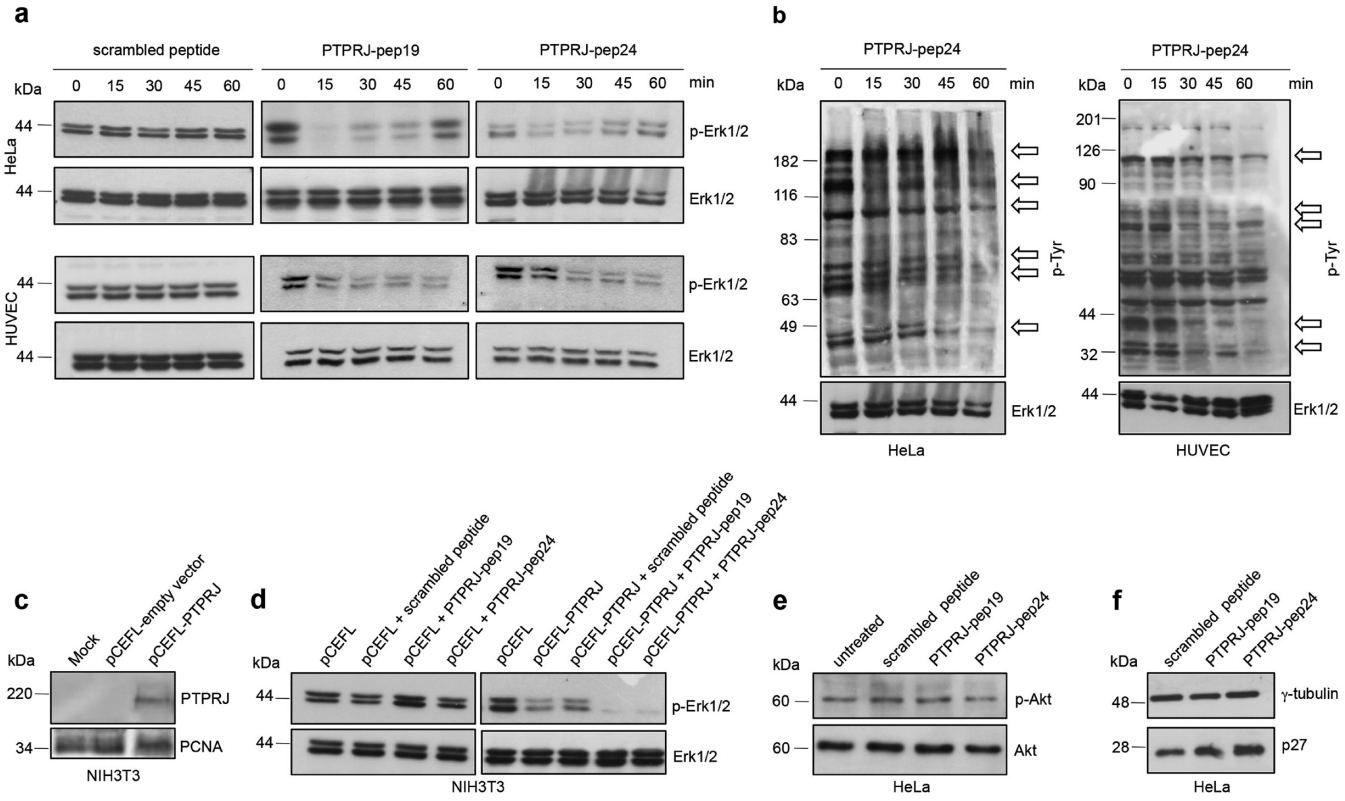

Figure 4. PTPRJ synthetic peptides suppress phosphorylation of both ERK1/2 and total phospho-tyrosine proteins and increase $p27^{Kip1}$ protein levels. HeLa and HUVEC cells were seeded in 6-well plates and 24 h later treated with 160 μM PTPRJ-pep19 and PTPRJ-pep24 or scrambled peptide for 0, 15, 30, 45, and 60 min. Cell lysates were subjected to immunoblots using (a) phospho-specific ERK1/2 (p-ERK) and (b) anti-phosphotyrosine antibodies. Blots were stripped and reprobed with total ERK1/2 as a loading control. (c) Western blot analysis of PTPRJ expression in protein extracts from NIH3T3 cells untransfected or transiently transfected with pCEFL-empty vector or pCEFL-PTPRJ. Expression was normalized by PCNA. (d) NIH3T3 cells were transfected with either pCEFL or pCEFL-PTPRJ and 24 h later were treated for 30 min with 160 μM PTPRJ-pep19 and PTPRJ-pep24 or scrambled peptide. Cell lysates were subjected to immunoblots using phospho-specific ERK1/2 (p-ERK), and then blots were stripped and reprobed with total ERK1/2 as a loading control. (e) HeLa cells were treated with 160 μM PTPRJ-pep19 and PTPRJ-pep24 or scrambled peptide for 30 min, and cell lysates were subjected to immunoblots using phospho-specific Akt (S473). Then the membrane section was stripped and blotted with total Akt to show equal protein loading. (f) HeLa cells were treated for 24 h with 160 μM PTPRJ-pep19 and PTPRJ-pep24 or scrambled peptide followed by 48 h recovery. Immunodetection was performed using anti-$p27^{Kip1}$ and anti-γ-tubulin specific antibodies.

Conversely, we observed a MAPK dephosphorylation in NIH3T3 cells transfected with a PTPRJ vector (pCEFL-PTPRJ) compared to their controls; the addition of PTPRJ-pep19 and PTPRJ-pep24 to NIH3T3/PTPRJ cells gave a higher extent of ERK dephosphorylation compared to both empty vector and NIH3T3/PTPRJ treated with scrambled peptide (Figure 4d, right panel).

As it has been demonstrated that Akt phosphorylation is downregulated by PTPRJ,[22] we evaluated Akt phosphorylation levels in HeLa cells treated with PTPRJ peptides; a Western blot probed with anti-phospho-Akt antibody showed that the phosphorylation extent of Akt was not reduced in HeLa cells treated with both PTPRJ-pep19 and PTPRJ-pep24 compared to the scrambled peptide or untreated cells (Figure 4e).

We previously demonstrated that PTPRJ activity was able to protect cell cycle inhibitor $p27^{Kip1}$ from its ubiquitin-mediated proteasome-dependent degradation in malignant cells, thus increasing its protein levels.[7] To check whether the administration of PTPRJ-pep19 and PTPRJ-pep24 could positively modulate $p27^{Kip1}$ protein, we treated HeLa cells as described above; both peptides induced a 3-fold increase of $p27^{Kip1}$ compared to scrambled peptide (Figure 4f).

Synthetic PTPRJ-Peptides Specifically Interact with Endogenous PTPRJ. To assess the ability of PTPRJ peptides to interact with endogenous PTPRJ on living cells, we used both HeLa cancer cells and HUVEC endothelial cells, both expressing detectable endogenous PTPRJ protein (Figure 3a), and binding specificity was assessed by flow cytometry. FITC-conjugated PTPRJ-pep24 bound HeLa cells in a dose-dependent manner (Figure 5a). We observed an increased mean fluorescence of HeLa cells by increasing the concentration of FITC-conjugated PTPRJ-pep24 (3, 6, 9 μg/mL), while fluorescence was unchanged in cells treated with equal amounts of control-FITC peptide (Figure 5b).

To verify the binding specificity of PTPRJ-peptides to PTPRJ, we expressed the human wild-type *PTPRJ* allele into NIH3T3 cells (Figure 4c), and we then examined the direct binding of peptides to cell surface by flow cytometry. PTPRJ overexpression in NIH3T3 (pCEFL-PTPRJ) confers PTPRJ-pep24 binding, which was detectable in a dose-dependent manner; conversely, no variations were observed in NIH3T3 transfected with the backbone vector (Figure 5c). Taken together, these data demonstrate that PTPRJ-pep24 gains the ability to bind the cell surface depending on PTPRJ expression.

dx.doi.org/10.1021/cb300281t | *ACS Chem. Biol.* 2012, 7, 1666–1676

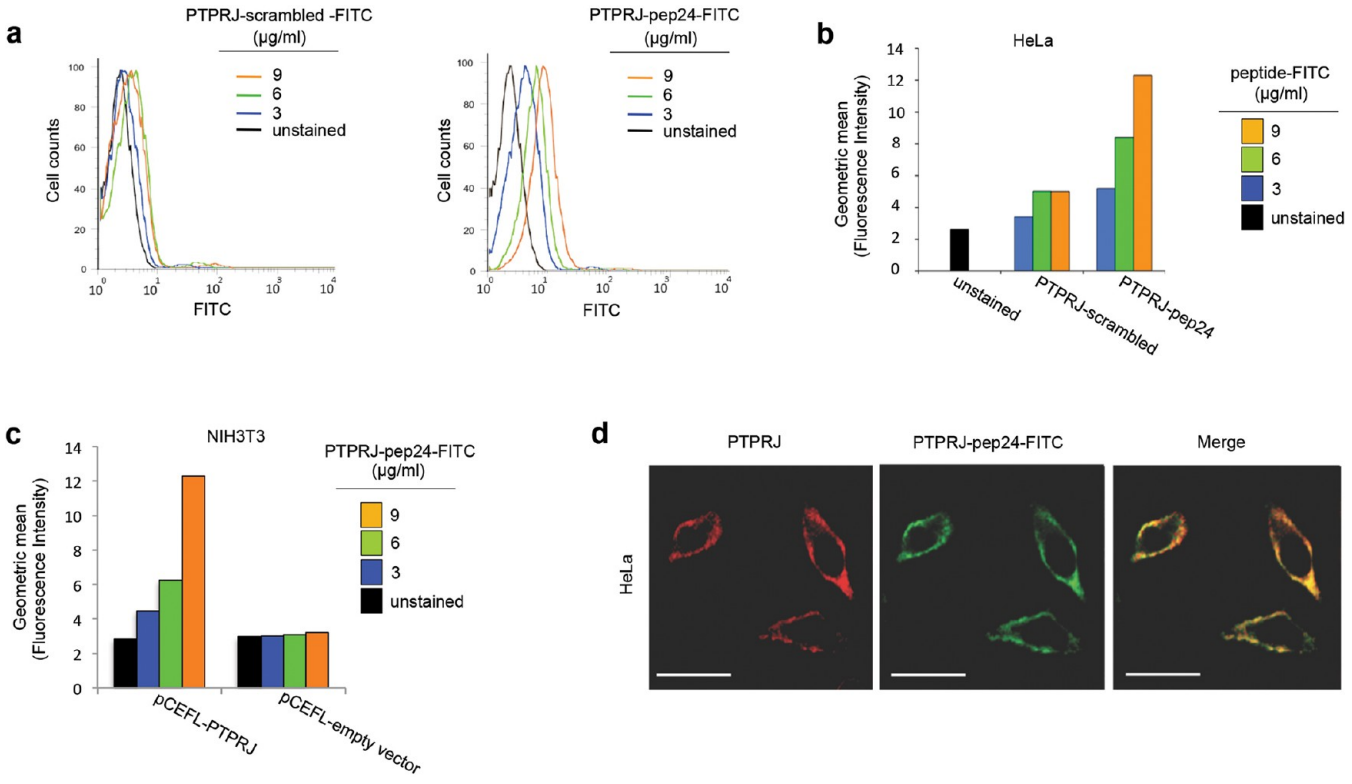

Figure 5. PTPRJ-pep24 peptide specifically binds and colocalizes with endogenous PTPRJ at cell surface. (a) HeLa cancer cells were incubated with FITC-conjugated PTPRJ-pep24 and FITC-conjugated scrambled peptides at 3 (blue line), 6 (green line), and 9 (orange line) μg/mL, and specific binding was analyzed by flow cytometry. (b) Geometric mean fluorescent intensity of PTPRJ-pep24 peptide was compared with that of scrambled peptide or autofluorescence (blue bar, 3 μg/mL; green bar 6 μg/mL; orange bar, 9 μg/mL; black bar, autofluorescence). (c) Geometric mean fluorescent intensity of PTPRJ-pep24 binding in NIH3T3 cells transfected with pCEFL-PTPRJ compared to transfected with the backbone vector. Flow-cytometric data were analyzed by FlowJo software. (d) Colocalization of FITC-conjugated pep24 with the surface PTPRJ. HeLa cells were cultured in eight-chamber slides, stained with either FITC-conjugated PTPRJ-pep24 (green) or antibody to PTPRJ (red), as described in Methods, and visualized by confocal microscopy. Merge of the images indicated the colocalization of PTPRJ-pep24 and PTPRJ. Scale bar =10 μm.

In addition, we observed by confocal microscopy that PTPRJ-pep24, used as a representative peptide, localizes on HeLa cells at plasma membrane; colocalization of this peptide with endogenous PTPRJ protein was also assessed (Figure 5d). These experiments confirmed that binding of PTPRJ-pep24 is linked to PTPRJ protein expression. Finally, a confocal microscopy analysis showed that PTPRJ-pep24 presented a prevalent plasma membrane distribution, which largely overlapped with distribution of endogenous PTPRJ.

Molecular Modeling of PTPRJ-Binding Peptides Suggests Supramolecular Aggregation States. PTPRJ-pep5, PTPRJ-pep19, PTPRJ-pep23, and PTPRJ-pep24 conformational search (see Methods for further details) reported for all compounds a large number of energy local minimum structures. Boltzmann population and clustering analysis highlighted several conformers separated by low energy barriers. With the aim to identify the most representative conformations of peptides, their MC ensembles were submitted to a clustering analysis[32] (Table S1 in Supporting Information). Results confirmed the MC search suggestions: all peptides showed a large number of clusters preventing a clear identification of the highly populated conformers. Conformations could move among their structural clusters with low variation in terms of internal energy. The graphical comparison of peptides global minimum energy conformers has not reported common chemical features useful to derive information related to their structure activity relationship (Figure S2 in Supporting Information). The large conformational variability and the residues of peptides suggested that they could be involved in aggregative processes. Moreover, taking into account that known PTPRJ ligands (*i.e.*, antibodies) report a chemical scaffold larger than these binders, we have addressed the target recognition to supramolecular aggregates of PTPRJ peptides. In order to evaluate such a possibility, docking simulations were carried out (Supporting Information for further details). These calculations, according to experimental data, indicated that all peptides were able to aggregate in stable omo-dimers (Figure 6). As described by thermodynamic analysis, the inactive peptides PTPRJ-pep5 and PTPRJ-pep23 dimers showed a stronger association with respect to the active PTPRJ-pep19 and PTPRJ-pep24 (Table S2 in Supporting Information).

NMR Analysis of PTPRJ-Interacting Peptides Indicates Their Aggregation in Solution. To explore the tendency of PTPRJ-pep5, PTPRJ-pep19, PTPRJ-pep23, and PTPRJ-pep24 to aggregate, these peptides were also investigated by solution NMR spectroscopy. NMR analysis was performed in water at different pH levels, temperatures, and concentrations. For peptides PTPRJ-pep19 and PTPRJ-pep24, the spectra showed splitting of the signals with a signal pattern (pattern 1) formed by sharp and intense signals and secondary patterns with broad signals. Following the signal pattern 1, complete ^{1}H NMR chemical shift assignments (Tables S3 and S4 in Supporting Information) were achieved according to the Wüthrich

dx.doi.org/10.1021/cb300281t | *ACS Chem. Biol.* 2012, 7, 1666–1676

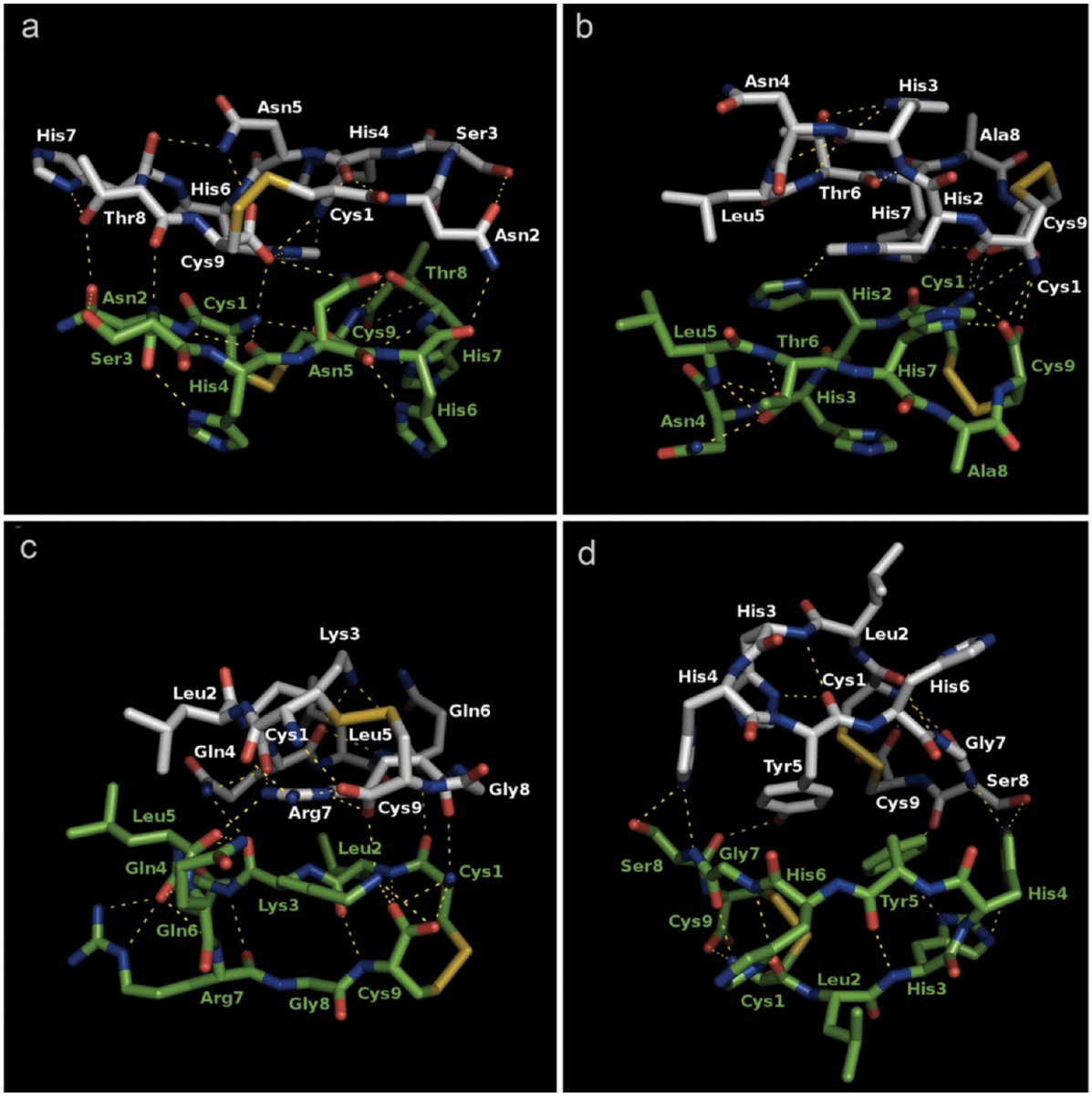

Figure 6. Global minimum energy structures of PTPRJ peptides. PTPRJ-pep5 (a), PTPRJ-pep19 (b), PTPRJ-pep23 (c), and PTPRJ-pep24 (d) omo-dimers. The two subunits of each complex are displayed in light gray and dark carbon colored polytubes, respectively. Dotted lines indicate hydrogen bonds.

procedure *via* the usual systematic application of TOCSY and NOESY experiments.[33] Considering this system, all NMR parameters indicated structural flexibility.

Considering the signals of the secondary patterns, these were broadened compared to the corresponding pattern 1, indicating that aggregation and/or chemical exchange phenomena occurred. For PTPRJ-pep19, H_a resonances of all residues but Thr[6] shift down-field (Figure S3 in Supporting Information), which could indicate a β-hairpin peptide folding with a turn structure encompassing residue 6. This is in accordance with the molecular modeling results and with the interatomic distances derived by the NOESY-NMR spectrum of PTPRJ-pep19 (Table S7 in Supporting Information). For PTPRJ-pep24, due to overlapping, only partial assignments of the secondary signal patterns could be achieved, and thus we were not able to formulate any hypothesis about the peptide structure in the supposed aggregate form. For PTPRJ-pep5 and PTPRJ-pep23, only broad signals were observed in the ^{1}H NMR spectra and only partial assignment could be done (Tables S5 and S6 in Supporting Information). This result indicated a higher tendency of these peptides to aggregation or chemical exchange phenomena.

To check the aggregation state of the peptides under the NMR conditions, DOSY experiments[34] were recorded. In fact, pulse field gradient NMR methods can be used to determine diffusion coefficients and from these the effective hydrodynamic radii of polypeptides. Moreover, empirical relationships between the hydrodynamic radius (R_h) and the number of residues (N) in a polypeptide were proposed.[35] The calculated hydrodynamic radii and number of residues of peptides PTPRJ-pep19, PTPRJ-pep23, and PTPRJ-pep24 (at 2 mM) are reported in Supporting Information in Table S8. Monomeric (N ~9, signal pattern 1) or dimeric (N ~18, secondary signal patterns) states were found for PTPRJ-pep19 and PTPRJ-

pep24. For PTPRJ-pep23, decay rates associated with any proton resonance pointed to higher aggregate states (on average, a trimer). Low solubility of PTPRJ-pep5 prevented obtaining good quality DOSY spectra for this peptide.

It is also possible that observed oligomers undergo chemical exchange with higher molecular weight aggregates that cannot be observed directly by solution state NMR methods since their NMR resonances are broadened beyond the detection level. To confirm this hypothesis STD-NMR experiments were also performed.[36] On-resonance irradiation induces higher intensity STD signals in the case of PTPRJ-pep5 and PTPRJ-pep23 compared to PTPRJ-pep19 and PTPRJ-pep24 (Table S8 and Figure S4 in Supporting Information) suggesting that high molecular weight aggregation states of the formers are present in solution.

Conclusions. Aberrant signaling from deregulated tyrosine kinase activity is a common feature of cancer cells, being a means by which they evade normal physiological constraints on growth and survival.[20] Thus, targeting kinases involved in cancer represents one of the major goals in the search for new and more effective anticancer drugs. The inhibition of tyrosine kinases is currently pursued by the use of (a) small molecules able to block their kinase activity by binding their catalytic domain and (b) antagonist monoclonal antibodies raised against the ectodomains of RTKs mutated in cancer.[37] Another intriguing approach to inhibit RTKs in cancer cells might be given by the activation of their physiological antagonists, such as protein tyrosine phosphatases.

PTPRJ, a receptor-type protein tyrosine phosphatase with tumor suppressor activity, dephosphorylates and inactivates several RTKs involved in cancer, such as PDGFR, HGFR/met, RET, EGFR, and VEGFR-2.[16−19,24]

The idea of PTPRJ as a candidate target for novel anticancer therapies is strongly supported by a study indicating that a PTPRJ monoclonal antibody is able to activate an inhibitory signal that hesitates in the negative modulation of MAPK phosphorylation, inhibition of both cell proliferation, and angiogenesis in an animal model.[28] However, although particularly encouraging, this task still represents a completely open field of investigations.

Targeted therapies by monoclonal antibodies are widely used in the treatment of a variety of human cancer;[38] however, they face several limitations to deal with. In fact, they show poor tumor penetration due to their size and are responsible for liver and bone marrow toxicity by nonspecific uptake.[39] Conversely, peptides represent much more interesting tools for the development of drugs to be used in clinical practice; they are considerably smaller than antibodies and should not trigger immune response even upon repeated administration.[40]

Although undefined components of the extracellular matrix can stimulate PTPRJ signaling,[41] as well as S2ED[26] and TSP1,[27] two PTPRJ ligands recently identified, the translation of these proteins into candidate therapeutic molecules is far from application. Here, we describe the identification of synthetic cyclic nonamer agonist peptides of PTPRJ. Their isolation was pursued by a cell-free screening of a combinatorial phage display library performed with a His-tagged PTPRJ recombinant protein. This represents a novel approach for the isolation of peptides binding transmembrane proteins, biopanning on whole intact cells being the way most frequently pursued for the identification of peptides from phage display libraries.[42−45] Cell surface molecules, including PTPRJ, are frequently post-translationally modified and because of that their native conformation cannot be obtained by using bacterial or insect hosts; thus, the best way to get a correct folding for a recombinant human protein would be its overexpression in human mammalian cells. For this reason, PTPRJ-His6 was overexpressed in a recipient human lung cell line (A549) through a recombinant adenovirus (Ad *PTPRJ*-His6) and then purified from cell membranes to perform the screening. While we did not get significant results through the biopanning, we isolated several phages with such a cell-free approach.

Synthetic PTPRJ peptides were tested in cancer cell cultures for the assessment of their biochemical and biological activities. Interestingly, the administration of two of them, PTPRJ-pep19 and PTPRJ-pep24, induced dramatic MAPK dephosphorylation, a critical mediator of mitogenic signals, and increased protein levels of $p27^{Kip1}$, a major player in cell cycle inhibition. Similarly, dephosphorylation of MAPK and cell growth inhibition was also observed in human primary endothelial HUVEC cells. However, biological effects, such as cell growth inhibition and apoptosis, did not parallel the extent of MAPK dephosphorylation and $p27^{Kip1}$ increase. This result might be explained by the low stability of the PTPRJ−peptide binding; however, although apparently not enthusiastic, chemical modifications of these peptides offer great possibilities of improvement in terms of biological effects.

Our data show concordance with results published by Takahashi and colleagues.[28] PTPRJ mAb effects were reached with the use of a bivalent PTPRJ antibody, whereas no effects were described with its monovalent form, suggesting that PTPRJ needs dimerization in order to activate its signaling; such a possibility was also recently underlined by our group.[46] Our study confirms the role of the peptide binder aggregation states onto the PTPRJ interaction. The biologically actives PTPRJ-pep19 and PTPRJ-pep24 revealed the capability to form stable dimer aggregates, while the inactives, PTPRJ-pep5 and PTPRJ-pep23, showed higher order aggregates, from trimers up. As a consequence we suggest that PTPRJ-pep19 and PTPRJ-pep24 dimer complexes are able to productively interact with PTPRJ, while higher order structures, reported for biologically inactive peptides, are too large for fitting the receptor.

Thus, the rationale of the use of PTPRJ peptides would consist in the stimulation of PTPRJ residual function in a large panel of cancer cells and in human tumors, where PTPRJ expression is dramatically impaired. Furthermore, the activity of PTPRJ peptides on proliferating endothelial cells proposes the fascinating perspective of a combined therapy able to target simultaneously both cell growth self-sufficiency and angiogenesis.

In conclusion, our results encourage a way to pursue in the near future for the generation of more active peptides to be tested *in vivo* in preclinical models of cancer. Molecular modeling, NMR structural analysis, and drug design studies might contribute to the generation of effective peptidomimetics to be used in cancer treatment.

METHODS

Cell Lines, Transfections, and Peptides. Both A549 lung cancer cells and HeLa cervical cancer cells were purchased from the American Type Culture Collection (ATCC). Cells were cultured in RPMI medium 1640 supplemented with 10% heat-inactivated FBS (Invitrogen). Human embryonic kidney HEK293 cells (Microbix), maintained in DMEM with 10% FBS, were used for generation and amplification of recombinant Ad *PTPRJ*-His6. Human umbilical vein

endothelial cells HUVEC (Clonetics) were cultured in M199 medium (Sigma-Aldrich) supplemented with 10% FBS, heparin (100 μg/mL; Sigma-Aldrich), and 10 ng/mL endothelial cell growth factor. Mouse fibroblast NIH3T3 cells (ATCC) were cultured in DMEM containing 10% FBS (Hyclone), L-glu, and pen/strep. pCEFL-*PTPRJ* and pCEFL-empty vector plasmids were transfected by LipofectAMINE 2000 (Invitrogen) (see Supporting Information for further details). Peptides were purchased from Invitrogen. The sequence of the scrambled peptide was CTLYHNAGC.

Selection and Amplification of PTPRJ-Binding Phages. Ph.D.-C7C Phage Display Peptide Library kit was purchased from New England Biolabs. PTPRJ-His6 protein was overexpressed in A549 by infecting 5×10^7 cells with Ad *PTPRJ*-His6 at a multiplicity of infection (MOI) of 25 (see Supporting Information for the generation of recombinant Ad *PTPRJ*-His6). Four days after infection, cell lysis was performed with Mem-PER Eukaryotic Membrane Protein Extraction Kit (Pierce) to enrich transmembrane proteins. PTPRJ-His6 protein was purified with Ni-NTA magnetic beads (Qiagen) following the manufacturer's protocols. Panning was performed by incubating PTPRJ-His6-coated beads with 3×10^{11} virions overnight at 4 °C. Beads were extensively washed with PBS with added 0.05% Tween-20 to remove unbound phages. PTPRJ-interacting phages were eluted with 0.2 M glycine-HCl (pH 2.2, 1 mg/mL BSA) followed by the addition of neutralizing solution (1 M Tris-HCl pH 9.1). Phages were titrated and amplified, and a second panning was performed with 1×10^{11}. Ultimately, four cycles of panning were performed. The binding of phages to PTPRJ was validated by an immunoscreening technique. Briefly, plaques of lysis from isolated phages were transferred to nitrocellulose filters, and membranes were blocked with PBS 1X, 0.1% NP-40; 5% milk; 0.02% NaN_3 and then incubated for 2 h at RT with 100 μg of purified PTPRJ-His6 protein. Filters were washed three times with a PBS 0.1% NP-40 solution and then probed with a monoclonal PTPRJ antibody (R&D Systems). After washing, membranes were hybridized with an alkaline phosphatase-conjugated anti-mouse IgG (Sigma-Aldrich) (dilution 1:5000) and then washed 6 times. Immunoreactive phage clones were detected by BCIP/NBT premixed substrate (Pierce); ultimately, 25 positive plaques were picked and expanded for further characterization. The specificity of individual peptide-display phage for PTPRJ-His6 binding was assessed by phage capture ELISA (see Supporting Information for details).

Mass Spectrometry. Peptide purity, as well as peptide cyclization and degradation over time, was assessed by matrix-assisted laser desorption ionization mass spectrometry (MALDI-MS) (see Supporting Information for technical details).

Antibodies and Western Blot Analysis. Goat polyclonal antibody against PTPRJ was purchased from R&D Systems. ERK1/2, phospho-ERK1/2, $p27^{Kip1}$, phospho-Tyr, and horseradish peroxidase (HRP)-conjugated anti-goat and anti-rabbit antibodies were purchased from Santa Cruz Biotechnology. Phospo-Akt (S473) and Akt antibodies were purchased from Cell Signaling (Cell Signaling Technology). Anti-γ-tubulin, anti-PCNA, and anti-GAPDH (all Santa Cruz Biotechnology) were used on each blot to ensure equal loading of protein on the gel.

Anti-penta-His monoclonal antibody was purchased from Qiagen. Cells were scraped into ice-cold phosphatase-buffered saline (PBS) and lysed in NP-40 lysis buffer containing 50 mM Tris-HCl pH 7.5, 150 mM NaCl, 1% NP-40, one protease inhibitor mixture tablet per 10 mL of buffer (Completet, Roche Diagnostics), 1 mM Na_3VO_4, and 50 mM NaF. Protein extraction and Western blotting procedures were previously described.[7]

Cell Survival Assay. To assess peptides-mediated inhibition of cell proliferation, HeLa and HUVEC cells were treated for 24 h with 160 μM PTPRJ-pep19 and PTPRJ-pep24 or control peptide followed by 48 h of recovery. After treatments cells were trypsinized and counted, and cell viability was determined by the trypan blue dye exclusion test. The results were expressed as percent variation in the number of viable cells treated with PTPRJ-peptides compared with control peptide-treated cells.

Cell Cycle Analysis and Apoptosis. Cells were plated at 0.5×10^6 cells/60 mm dish and treated for 72 h with 160 μM PTPRJ-pep19 and PTPRJ-pep24 peptides. Cells were harvested and fixed with cold 70% ethanol. Before analysis, cells were washed with PBS and stained with a solution containing 50 μg/mL propidium iodide, 250 μg/mL RNase, and 0.04% Nonidet P40 (NP-40) for 30 min at RT in the dark. The fluorescence of stained cells was analyzed by flow cytometry using a FACS Caliber (Becton Dickinson, San Jose, CA). A flow cytometric sub-G_0-G_1 peak was detected on DNA plots using the CellQuest software according to the Modfit model (Becton Dickinson).

TdT-mediated dUTP-biotin nick end labeling (TUNEL) assay was performed in HeLa cells by using Mebstain Apoptosis TUNEL Kit direct according to the manufacturer's instructions (MBL International). The percentages of TUNEL-positive cells were determined by flow cytometry using FACSCan (BD Biosciences). Data were analyzed by using FlowJo software (Tree Star).

Caspase proteolytic processing was analyzed by Western blotting using a 1:5000 dilution of Ab to caspase-3 (Cell Signaling Technology) followed by chemiluminescence and autoradiography.

Fluorescence-Activated Cell Sorting Analysis. To verify the specific binding of PTPRJ-pep19 and PTPRJ-pep24 peptides to PTPRJ in HeLa cells, 2.5×10^4 cells were chilled on ice for 5 min and incubated for 30 min at 4 °C with FITC-labeled PTPRJ-pep19 and PTPRJ-pep24 or FITC-labeled nonavid peptide at the final concentration of 3, 6, or 9 μg/mL. Cells were centrifuged at 1500 rpm for 3 min, the supernatant was discarded, and cells were resuspended in 500 μL of PBS. The binding of PTPRJ-pep19 and PTPRJ-pep24 peptides was also assayed on NIH3T3 cells, a Ptprj-negative cell line, after transfection with either pCEFL-*PTPRJ* or pCEFL, used as a control. Briefly, cells were blocked with 1% BSA 1X PBS, washed, and incubated for 20 min with PTPRJ primary antibody (R&D), followed by incubation with PE-conjugated secondary antibody. After washing, NIH3T3 cells were incubated with 3, 6, or 9 μg/mL of FITC-labeled peptides. Samples were analyzed with FACSCan instruments (Becton Dickinson), and data were analyzed by using FlowJo software (Tree Star).

Immunofluorescence. HeLa cells were placed onto slides and allowed to settle for 24 h. Then, cells were incubated with FITC-conjugated PTPRJ-pep24 (50 μg/mL) for 10 min at 4 °C, washed in 1% BSA 1X PBS, and fixed with 4% *p*-formaldehyde for 15 min at 4 °C. After extensive washing, cells were blocked in 1% BSA 1X PBS, incubated with mouse mAb to PTPRJ followed by PE-conjugated anti-mouse secondary antibody. Finally, cells were prepared with mounting medium (ProLong antifade, Invitrogen) under coverslip and visualized by confocal microscopy.

Molecular Modeling. Theoretical 3D models of PTPRJ-pep5, PTPRJ-pep19, PTPRJ-pep23, and PTPRJ-pep24 were built using Maestro ver. 9.1 GUI,[47] and the conformational properties were explored by means of Monte Carlo (MC) search. Aggregation processes were investigated using our in house docking software MolInE[48,49] for generating bimolecular complexes (see Supporting Information for details).

NMR Spectroscopy. NMR spectra were recorded on a Varian INOVA 700 MHz spectrometer equipped with a *z*-gradient 5 mm triple-resonance probe head. DOSY-NMR[34] were performed to determine the oligomeric state of the peptides using an internal standard method.[35] STD-NMR[36] experiments were performed with on-resonance and off-resonance saturation at $\delta = -2$ and $\delta = -16$ ppm, respectively. A detailed description of NMR spectroscopy experiments is available in Supporting Information.

■ ASSOCIATED CONTENT

Ⓢ Supporting Information

This material is available free of charge *via* the Internet at http://pubs.acs.org.

■ AUTHOR INFORMATION

Corresponding Author

*E-mail: trapasso@unicz.it.

Notes

The authors declare no competing financial interest.

■ ACKNOWLEDGMENTS

The present study was supported by a grant from the Associazione Italiana Ricerca Cancro (AIRC). F.P. was a recipient of a FIRC (Fondazione Italiana Ricerca Cancro) fellowship.

■ REFERENCES

(1) Alonso, A., Sasin, J., Bottini, N., Friedberg, I., Friedberg, I., Osterman, A., Godzik, A., Hunter, T., Dixon, J., and Mustelin, T. (2004) Protein tyrosine phosphatases in the human genome. *Cell 117*, 699−711.

(2) Ostman, A., Hellberg, C., and Böhmer, F. D. (2006) Protein-tyrosine phosphatases and cancer. *Nat. Rev. Cancer 6*, 307−320.

(3) Honda, H., Inazawa, J., Nishida, J., Yazaki, Y., and Hirai, H. (1994) Molecular cloning, characterization, and chromosomal localization of a novel protein-tyrosine phosphatase, HPTP eta. *Blood 84*, 4186−4194.

(4) Ostman, A., Yang, Q., and Tonks, N. K. (1994) Expression of DEP-1, a receptor-like protein-tyrosine-phosphatase, is enhanced with increasing cell density. *Proc. Natl. Acad. Sci. U.S.A. 91*, 9680−9684.

(5) Keane, M. M., Lowrey, G. A., Ettenberg, S. A., Dayton, M. A., and Lipkowitz, S. (1996) The protein tyrosine phosphatase DEP-1 is induced during differentiation and inhibits growth of breast cancer cells. *Cancer Res. 56*, 4236−4243.

(6) Zhang, L., Martelli, M. L., Battaglia, C., Trapasso, F., Tramontano, D., Viglietto, G., Porcellini, A., Santoro, M., and Fusco, A. (1997) Thyroid cell transformation inhibits the expression of a novel rat protein tyrosine phosphatase. *Exp. Cell. Res. 235*, 62−70.

(7) Trapasso, F., Iuliano, R., Boccia, A., Stella, A., Visconti, R., Bruni, P., Baldassarre, G., Santoro, M., Viglietto, G., and Fusco, A. (2000) Rat protein tyrosine phosphatase eta suppresses the neoplastic phenotype of retrovirally transformed thyroid cells through the stabilization of p27(Kip1). *Mol. Cell. Biol. 20*, 9236−9246.

(8) Paduano, F., Dattilo, V., Narciso, D., Bilotta, A., Gaudio, E., Menniti, M., Agosti, V., Palmieri, C., Perrotti, N., Fusco, A., Trapasso, F., and Iuliano, R. (2012) Protein tyrosine phosphatase PTPRJ is negatively regulated by microRNA-328. *FEBS J.*, May 7 DOI: 10.1111/j.1742-4658.2012.08624.x.

(9) Iuliano, R., Trapasso, F., Le Pera, I., Schepis, F., Samà, I., Clodomiro, A., Dumon, K. R., Santoro, M., Chiarotti, L., Viglietto, G., and Fusco, A. (2003) An adenovirus carrying the rat protein tyrosine phosphatase eta suppresses the growth of human thyroid carcinoma cell lines in vitro and in vivo. *Cancer Res. 63*, 882−886.

(10) Trapasso, F., Yendamuri, S., Dumon, K. R., Iuliano, R., Cesari, R., Feig, B., Seto, R., Infante, L., Ishii, H., Vecchione, A., During, M. J., Croce, C. M., and Fusco, A. (2004) Restoration of receptor-type protein tyrosine phosphatase eta function inhibits human pancreatic carcinoma cell growth in vitro and in vivo. *Carcinogenesis 25*, 2107−2114.

(11) Ruivenkamp, C. A., van Wezel, T., Zanon, C., Stassen, A. P., Vlcek, C., Csikós, T., Klous, A. M., Tripodis, N., Perrakis, A., Boerrigter, L., Groot, P. C., Lindeman, J., Mooi, W. J., Meijjer, G. A., Scholten, G., Dauwerse, H., Paces, V., van Zandwijk, N., van Ommen, G. J., and Demant, P. (2002) Ptprj is a candidate for the mouse colon-cancer susceptibility locus Scc1 and is frequently deleted in human cancers. *Nat. Genet. 31*, 295−300.

(12) Ruivenkamp, C., Hermsen, M., Postma, C., Klous, A., Baak, J., Meijer, G., and Demant, P. (2003) LOH of PTPRJ occurs early in colorectal cancer and is associated with chromosomal loss of 18q12−21. *Oncogene 22*, 3472−3474.

(13) Iuliano, R., Le Pera, I., Cristofaro, C., Baudi, F., Arturi, F., Pallante, P., Martelli, M. L., Trapasso, F., Chiariotti, L., and Fusco, A. (2004) The tyrosine phosphatase PTPRJ/DEP-1 genotype affects thyroid carcinogenesis. *Oncogene 23*, 8432−8438.

(14) Trapasso, F., Drusco, A., Costinean, S., Alder, H., Aqeilan, R. I., Iuliano, R., Gaudio, E., Raso, C., Zanesi, N., Croce, C. M., and Fusco, A. (2006) Genetic ablation of Ptprj, a mouse cancer susceptibility gene, results in normal growth and development and does not predispose to spontaneous tumorigenesis. *DNA Cell Biol. 25*, 376−382.

(15) Zhu, J. W., Brdicka, T., Katsumoto, T. R., Lin, J., and Weiss, A. (2008) Structurally distinct phosphatases CD45 and CD148 both regulate B cell and macrophage immunoreceptor signaling. *Immunity 28*, 183−196.

(16) Kovalenko, M., Denner, K., Sandström, J., Persson, C., Gross, S., Jandt, E., Vilella, R., Böhmer, F., and Ostman, A. (2000) Site-selective dephosphorylation of the platelet-derived growth factor beta-receptor by the receptor-like protein-tyrosine phosphatase DEP-1. *J. Biol. Chem. 275*, 16219−16226.

(17) Palka, H. L., Park, M., and Tonks, N. K. (2003) Hepatocyte growth factor receptor tyrosine kinase met is a substrate of the receptor protein-tyrosine phosphatase DEP-1. *J. Biol. Chem. 278*, 5728−5735.

(18) Iervolino, A., Iuliano, R., Trapasso, F., Viglietto, G., Melillo, R. M., Carlomagno, F., Santoro, M., and Fusco, A. (2006) The receptor-type protein tyrosine phosphatase J antagonizes the biochemical and biological effects of RET-derived oncoproteins. *Cancer Res. 66*, 6280−6287.

(19) Berset, T. A., Hoier, E. F., and Hajnal, A. (2005) The C. elegans homolog of the mammalian tumor suppressor Dep-1/Scc1 inhibits EGFR signaling to regulate binary cell fate decisions. *Genes Dev. 19*, 1328−1340.

(20) Hanahan, D., and Weinberg, R. A. (2000) The hallmarks of cancer. *Cell 100*, 57−70.

(21) Baker, J. E., Majeti, R., Tangye, S. G., and Weiss, A. (2001) Protein tyrosine phosphatase CD148-mediated inhibition of T-cell receptor signal transduction is associated with reduced LAT and phospholipase Cgamma1 phosphorylation. *Mol. Cell. Biol. 21*, 2393−2403.

(22) Omerovic, J., Clague, M. J., and Prior, I. A. (2010) Phosphatome profiling reveals PTPN2, PTPRJ and PTEN as potent negative regulators of PKB/Akt activation in Ras-mutated cancer cells. *Biochem. J. 426*, 65−72.

(23) Tsuboi, N., Utsunomiya, T., Roberts, R. L., Ito, H., Takahashi, K., Noda, M., and Takahashi, T. (2008) The tyrosine phosphatase CD148 interacts with the p85 regulatory subunit of phosphoinositide 3-kinase. *Biochem. J. 413*, 193−200.

(24) Lampugnani, G. M., Zanetti, A., Corada, M., Takahashi, T., Balconi, G., Breviario, F., Orsenigo, F., Cattelino, A., Kemler, R., Daniel, T. O., and Dejana, E. (2003) Contact inhibition of VEGF-induced proliferation requires vascular endothelial cadherin, beta-catenin, and the phosphatase DEP-1/CD148. *J. Cell Biol. 161*, 793−804.

(25) Chabot, C., Spring, K., Gratton, J. P., Elchebly, M., and Royal, I. (2009) New role for the protein tyrosine phosphatase DEP-1 in Akt activation and endothelial cell survival. *Mol. Cell. Biol. 29*, 241−53.

(26) Whiteford, J. R., Xian, X., Chaussade, C., Vanhaesebroeck, B., Nourshargh, S., and Couchman, J. R. (2011) Syndecan-2 is a novel ligand for the protein tyrosine phosphatase receptor CD148. *Mol. Biol. Cell 22*, 3609−24.

(27) Takahashi, K., Mernaugh, R. L., Friedman, D. B., Weller, R., Tsuboi, N., Yamashita, H., Quaranta, V., and Takahashi, T. (2012) Trombospondin-1 acts as a ligand for CD148 tyrosine phosphatase. *Proc. Natl. Acad. Sci. U.S.A. 109*, 1985−90.

(28) Takahashi, T., Takahashi, K., Mernaugh, R. L., Tsuboi, N., Liu, H., and Daniel, T. O. (2006) A monoclonal antibody against CD148, a receptor-like tyrosine phosphatase, inhibits endothelial-cell growth and angiogenesis. *Blood 108*, 1234−1242.

(29) Barry, M. A., Dower, W. J., and Johnston, S. A. (1996) Toward cell-targeting gene therapy vectors: selection of cell-binding peptides from random peptide-presenting phage libraries. *Nat. Med. 2*, 299−305.

(30) Giordano, R. J., Cardó-Vila, M., Lahdenranta, J., Pasqualini, R., and Arap, W. (2001) Biopanning and rapid analysis of selective interactive ligands. *Nat. Med. 7*, 1249−1253.
(31) Sacco, F., Tinti, M., Palma, A., Ferrari, E., Nardozza, A. P., Hooft van Huijsduijnen, R., Takahashi, T., Castagnoli, L., and Cesareni, G. (2009) Tumor suppressor density-enhanced phosphatase-1 (DEP-1) inhibits the RAS pathway by direct dephosphorylation of ERK1/2 kinases. *J. Biol. Chem. 284*, 22048−22058.
(32) Daura, X., Gademann, K., Jaun, B., Seebach, D., van Gunsteren, W. F., and Mark, A. E. (1999) Peptide folding: When simulation meets experiment. *Angew. Chem. Int. 38*, 236−40.
(33) Wüthrich, K. (1986) *NMR of Proteins and Nucleic Acids*, John Wiley & Sons, Inc., New York.
(34) Wu, D., Chen, A., and Johnson, C. S. (1995) An improved diffusion-ordered spectroscopy experiment incorporating bipolar-gradient pulses. *J. Magn. Reson. Ser. A 115*, 260−264.
(35) Wilkins, D. K., Grimshaw, S. B., Receveur, V., Dobson, C. M., Jones, J. A., and Smith, L. J. (1999) Hydrodynamic radii of native and denatured proteins measured by pulse field gradient NMR techniques. *Biochemistry 38*, 16424−16431.
(36) Mayer, M., and Meyer, B. (1999) Characterization of ligand binding by saturation transfer difference NMR spectroscopy. *Angew. Chem., Int. Ed. 38*, 1784−1788.
(37) Zhang, J., Yang, P. L., and Gray, N. S. (2009) Targeting cancer with small molecule kinase inhibitors. *Nat. Rev. Cancer 9*, 28−39.
(38) Gschwind, A., Fischer, O. M., and Ullrich, A. (2004) The discovery of receptor tyrosine kinases: targets for cancer therapy. *Nat. Rev. Cancer 4*, 361−370.
(39) Reilly, R. M., Sandhu, J., Alvarez-Diez, T. M., Gallinger, S., Kirsh, J., and Stern, H. (1995) Problems of delivery of monoclonal antibodies. Pharmaceutical and pharmacokinetic solutions. *Clin. Pharmacokinet. 28*, 126−142.
(40) Aina, O. H., Sroka, T. C., Chen, M. L., and Lam, K. S. (2002) Therapeutic cancer targeting peptides. *Biopolymers 66*, 184−199.
(41) Sörby, M., Sandström, J., and Ostman, A. (2001) An extracellular ligand increases the specific activity of the receptor-like protein tyrosine phosphatase DEP-1. *Oncogene 20*, 5219−5224.
(42) Ballinger, M. D., Shyamala, V., Forrest, L. D., Deuter-Reinhard, M., Doyle, L. V., Wang, J. X., Panganiban-Lustan, L., Stratton, J. R., Apell, G., Winter, J. A., Doyle, M. V., Rosenberg, S., and Kavanaugh, W. M. (1999) Semirational design of a potent, artificial agonist of fibroblast growth factor receptors. *Nat. Biotechnol. 17*, 1199−1204.
(43) Cwirla, S. E., Balasubramanian, P., Duffin, D. J., Wagstrom, C. R., Gates, C. M., Singer, S. C., Davis, A. M., Tansik, R. L., Mattheakis, L. C., Boytos, C. M., Schatz, P. J., Baccanari, D. P., Wrighton, N. C., Barrett, R. W., and Dower, W. J. (1997) Peptide agonist of the thrombopoietin receptor as potent as the natural cytokine. *Science 276*, 1696−1699.
(44) Wrighton, N. C., Farrell, F. X., Chang, R., Kashyap, A. K., Barbone, F. P., Mulcahy, L. S., Johnson, D. L., Barrett, R. W., Jolliffe, L. K., and Dower, W. J. (1996) Small peptides as potent mimetics of the protein hormone erythropoietin. *Science 273*, 458−464.
(45) Zhao, P., Grabinski, T., Gao, C., Skinner, R. S., Giambernardi, T., Su, Y., Hudson, E., Resau, J., Gross, M., Vande Woude, G. F., Hay, R., and Cao, B. (2007) Identification of a met-binding peptide from a phage display library. *Clin. Cancer Res. 13*, 6049−6055.
(46) Iuliano, R., Raso, C., Quintiero, A., Le Pera, I. L., Pichiorri, F., Palumbo, T., Palmieri, D., Pattarozzi, A., Florio, T., Viglietto, G., Trapasso, F., Croce, C. M., and Fusco, A. (2009) The eighth fibronectin type III domain of protein tyrosine phosphatase receptor J influences the formation of protein complexes and cell localization. *J. Biochem. 145*, 377−385.
(47) Schrödinger, L.L.C., New York, NY (2010); www.schrodinger.com
(48) Alcaro, S., Gasparrini, F., Incani, O., Mecucci, S., Misiti, D., Pierini, M., and Villani, C. (2000) A "quasi-flexible" automatic docking processing for studying stereoselective recognition mechanisms. Part I. Protocol validation. *J. Comput. Chem. 21*, 515−530.
(49) Alcaro, S., Gasparrini, F., Incani, O., Caglioti, L., Pierini, M., and Villani, C. (2007) "Quasi flexible" automatic docking processing for studying stereoselective recognition mechanisms, Part 2: Prediction of $\Delta\Delta G$ of complexation and ^{1}H-NMR NOE correlation. *J. Comput. Chem. 28*, 1119−1128.